Aperture Maximization with Half-Wavelength Spacing, via a 2-Circle Concentric Array Geometry that is Uniform but Sparse

Musyoka KINYILI, Dominic Makaa KITAVI and Cyrus Gitonga NGARI
Department of Mathematics, Computing, and Information Technology,
University of Embu, Embu, Kenya.

***Abstract*— This paper proposes a new sensor-array geometry (the 2-circle concentric array geometry), that maximizes the array's spatial aperture mainly for bivariate azimuth-polar resolution of direction-of-arrival estimation problem. The proposed geometry provides almost invariant azimuth angle coverage and offers the advantage of full rotational symmetry (circular invariance) while maintaining an inter-sensor spacing of only an half wavelength (for non-ambiguity with respect to the Cartesian direction cosines). A better-accurate performance in direction finding of the proposed array grid over a single ring array geometry termed as uniform circular array (UCA) is hereby analytically verified via Cramér-Rao bound analysis. Further, the authors demonstrate that the proposed sensor-array geometry has better estimation accuracy than a single ring array.**

***Index Terms*— antenna arrays, array signal processing, direction-of-arrival estimation, parameter estimation, planar circular arrays.**

I Introduction

The problem of estimating angle-of-arrival (AoA) of a plane wave (or multiple plane waves) is commonly referred to as direction finding (DF) or direction-of-arrival (DoA) estimation problem [1]. DF finds its application in radar, sonar, medical diagnosis and treatment, electronic surveillance, radio astronomy [2], position location and tracing systems [3]. This is simply because it is a major method of location determination, in security services especially by reconnaissance of radio communications of criminal organization and in military intelligence by detecting activities of potential enemies and gaining information on enemy's communication order [4]. Due to its diverse application and difficulty of obtaining the optimum estimator, the topic has attracted a significant amount of attention over the last several decades.

Several algorithms exist to address the problem of estimating azimuth-polar AoA of multiple sources using the signal received at the array of sensors [5]. Some of the already used methods of DF are: Maximum likelihood (ML) [6], MUSIC (MUltiple SIgnal Classification) which is a highly popular eigenstructure-based direction-of-arrival estimation problem method applicable to a non-uniformly spaced array of sensors [7], [8], ESPRIT (Estimation of Signal Parameters via Rotational Invariance Technique) [9], Cramér-Rao Bound (CRB) which has been found to be the most accurate technique in DF and the simplest due to its simplicity in computations [10], and other techniques. To achieve DF, elements termed as antennas or sensors are used. These sensors are either randomly distributed or arranged in a desired geometric pattern mainly to improve the estimation performance. Some of the geometric patterns which have been used include: Uniform linear array (ULA), uniform circular array (UCA), uniform rectangular array (URA) [1], regular tetrahedral array, collocated triad of orthogonal dipoles [11], and L-shaped 2-dimensional array [12], [13].

Of all array geometries, circular and concentric circular arrays alone provides almost invariant azimuth angle coverage and offers full rotational symmetry about the origin, thereby realizing azimuthal invariance (with the azimuth defined on the circular plane) as well as increasing array's spatial aperture [8], [14]–[20]. Furthermore, a sensor-array's spatial resolution in the azimuth and polar, increases with the size of the array's aperture. As evidenced in [21]–[24], recent research has focused on strategies to enlarge this aperture without additional sensors. However, one difficult on widening array's aperture is to avoid side and grating lobes in beam-forming and also to avoid cyclic ambiguities in direction finding [14], [25]–[28]; these problems would be encountered if the inter-sensor spacing exceeds half a wavelength, thereby violating the spatial version of the Nyquist sampling theorem [18], [29]–[32]. This now raises an alarming question that, how then may the circular array aperture be widened without additional (isotropic) sensors while maintaining half-wavelength inter-sensor spacing? The inter-sensor spacing here equals $2R\sin\left(\frac{\pi}{L}\right)$, where L and R denotes the number of isotropic sensors on the circumference of a circle and the radius respectively.

As aforementioned, a new concentric circular array grid termed as 2-circle concentric array geometry or concentric uniform circular array (CUCA) geometry, that maintains an inter-sensor spacing of only half a wavelength (to avoid ambiguity in the estimated direction-of-arrival), that provides almost invariant azimuth angle coverage and retains the advantage of full rotational symmetry, and that maximizes the array's spatial aperture, with only a small increase in the number of sensors is proposed. Furthermore, the paper presents derivation of the Cramér-Rao bound for the proposed array grid and compares the performance of the proposed array grid and that of a single ring grid in direction finding.

Finally, the paper is organized into five sections in which Section I is the introduction, Section II presents array manifold, Section III presents the Cramér-Rao bound derivation, Section IV presents the results analysis and discussion, and Section V gives conclusion.

II ARRAY MANIFOLD

II-A. A Uniform Circular Array (UCA) of Isotropic Sensors

Consider a circle centered at the Cartesian origin and of radius R_{UCA}. Suppose L_{UCA} number of isotropic sensors are uniformly spaced on the circle. See Figure 1.

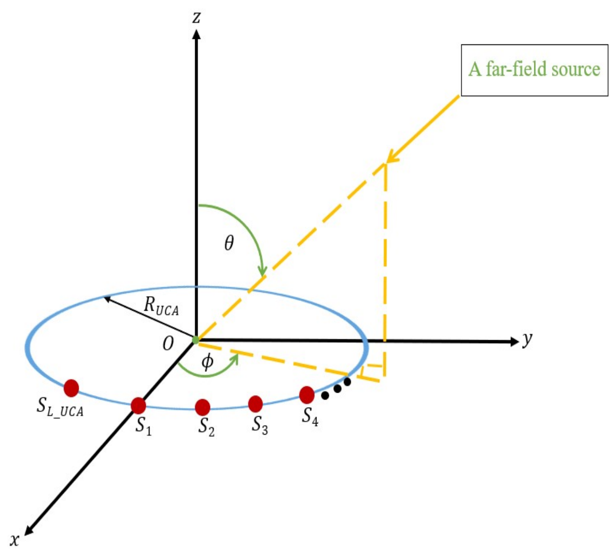

Fig. 1. A uniform circular array of isotropic sensors.

The position of the ℓ^{th} sensor is

$$p_\ell = \left[R_{\text{UCA}} \cos \frac{2\pi(\ell-1)}{L_{\text{UCA}}}, R_{\text{UCA}} \sin \frac{2\pi(\ell-1)}{L_{\text{UCA}}}, 0 \right]^T, \quad (1)$$

for $\ell = 1, 2, 3, \cdots, L_{\text{UCA}}$, where ^{T} denotes transposition; and the ℓ^{th} entry of the $L_{\text{UCA}} \times 1$ array manifold vector is [1], [10], [33]–[35]

$$\begin{aligned} & [\mathbf{a}_{\text{UCA}}(\theta, \phi)]_\ell \\ = \; & \exp\left\{ j \frac{2\pi R_{\text{UCA}}}{\lambda} \sin(\theta) \cos\left(\phi - \frac{2\pi(\ell-1)}{L_{\text{UCA}}} \right) \right\} \end{aligned} \quad (2)$$

where $\theta \in \left[0, \frac{\pi}{2}\right]$, $\phi \in [0, 2\pi)$, and λ is the wavelength which is a prior known deterministic constant.

II-B. Concentric Uniform Circular Array (CUCA) of Isotropic Sensors

Consider two concentric circles of radii R_{in} and R_{out}, both centered at the Cartesian origin and on the x-y plane, as illustrated in Figure 2.

Let L_{in} and L_{out} denote the number of isotropic sensors placed on the inner and the outer circles respectively.

This 2-circle concentric array has an array manifold of

$$\mathbf{a}(\theta, \phi) = \begin{bmatrix} \mathbf{a}_{\text{in}}(\theta, \phi) \\ \mathbf{a}_{\text{out}}(\theta, \phi) \end{bmatrix}, \quad (3)$$

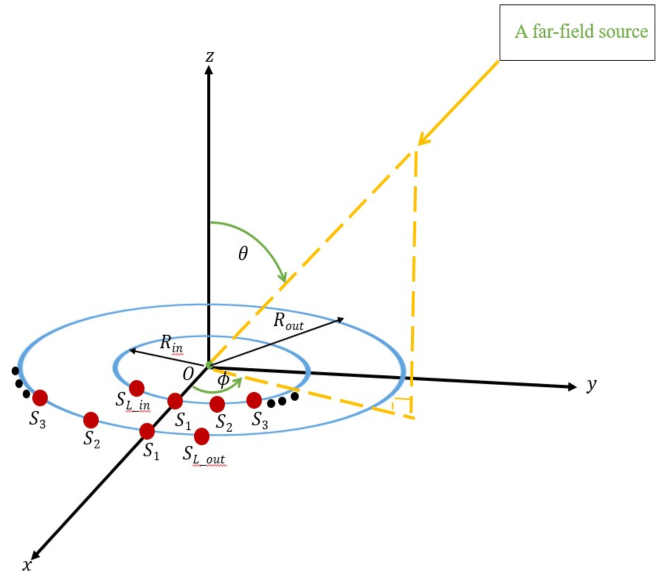

Fig. 2. A 2-circle concentric array.

where

$$\begin{aligned} & [\mathbf{a}_{\text{in}}(\theta, \phi)]_{\ell_{\text{in}}} \\ = \; & \exp\left\{ j \frac{2\pi R_{\text{in}}}{\lambda} \sin(\theta) \cos\left(\phi - \frac{2\pi(\ell_{\text{in}}-1)}{L_{\text{in}}} \right) \right\} \end{aligned} \quad (4)$$

and

$$\begin{aligned} & [\mathbf{a}_{\text{out}}(\theta, \phi)]_{\ell_{\text{out}}} \\ = \; & \exp\left\{ j \frac{2\pi R_{\text{out}}}{\lambda} \sin(\theta) \cos\left(\phi - \frac{2\pi(\ell_{\text{out}}-1)}{L_{\text{out}}} \right) \right\} \end{aligned} \quad (5)$$

In (4)-(5), $\ell_{\text{in}} = 1, 2, \cdots, L_{\text{in}}$; and $\ell_{\text{out}} = 1, 2, \cdots, L_{\text{out}}$.

III Cramér-Rao Bound (CRB) Derivation

III-A. The Data Model

Suppose the data is corrupted by additive noise. Then, the observed data is

$$\mathbf{x}(m) \quad = \quad \mathbf{a}(\theta,\phi)s(m) + \mathbf{n}(m) \tag{6}$$

where, $s(m)$ is the incident signal at time instant m and $\mathbf{n}(m)$ is additive complex-valued spatio-temporal white Gaussian noise with a mean of zero and a variance of σ_n^2 which are both prior known [1], [5], [8], [11], [13], [34]–[43].

Consider M number of discrete-time samples, then (6) can be represented as

$$\mathbf{x} \quad = \quad \mathbf{s}\otimes\mathbf{a}(\theta,\phi) + \mathbf{n} \tag{7}$$

where

$$\begin{aligned}\mathbf{x} &:= \left[[\mathbf{x}(1)]^T,\ [\mathbf{x}(2)]^T, \cdots, [\mathbf{x}(M)]^T\right]^T, \\ \mathbf{s} &:= \left[s(1),\ s(2), \cdots, s(M)\right]^T, \\ \mathbf{n} &:= \left[[\mathbf{n}(1)]^T,\ [\mathbf{n}(2)]^T, \cdots, [\mathbf{n}(M)]^T\right]^T,\end{aligned}$$

denote the observations, the complex-valued incident signal, and the additive noise, respectively. Moreover, $\otimes$ and ^{T}, denote the Kronecker product and the transposition, respectively [11], [13], [35], [42].

The data's probability distribution function (PDF) is,

$$p(\mathbf{x}|\theta,\phi) \quad = \quad \frac{1}{\sqrt{|2\pi\boldsymbol{\Gamma}|}}\left\{-\frac{1}{2}\left[\mathbf{x}-\boldsymbol{\mu}\right]^H\boldsymbol{\Gamma}^{-1}\left[\mathbf{x}-\boldsymbol{\mu}\right]\right\} \tag{8}$$

where

$$\begin{aligned}\boldsymbol{\mu} &:= E[\mathbf{x}] \\ &= \mathbf{s}\otimes\mathbf{a}(\theta,\phi), \qquad (9)\\ \boldsymbol{\Gamma} &:= E\left\{[\mathbf{x}-\boldsymbol{\mu}][\mathbf{x}-\boldsymbol{\mu}]^H\right\} \\ &= \sigma_n^2\mathbf{I}_{(L_{\text{in}}+L_{\text{out}})M}, \qquad (10)\end{aligned}$$

and $\mathbf{I}_{(L_{\text{in}}+L_{\text{out}})M}$ denotes an identity matrix of size $(L_{\text{in}}+L_{\text{out}})M \times (L_{\text{in}}+L_{\text{out}})M$.

III-B. The Fisher Information Matrix (FIM)

Recall that the observed data vector is complex-valued hence, the Fisher Information matrix (FIM) has a $(k,n)^{th}$ entry of

$$\begin{aligned}[\mathbf{F}(\xi)]_{k,n} &= 2\text{Re}\left\{\left[\frac{\partial\boldsymbol{\mu}}{\partial\xi_k}\right]^H\boldsymbol{\Gamma}^{-1}\frac{\partial\boldsymbol{\mu}}{\partial\xi_n}\right\} \\ &\quad +\text{Tr}\left\{\boldsymbol{\Gamma}^{-1}\frac{\partial\boldsymbol{\Gamma}}{\partial\xi_k}\boldsymbol{\Gamma}^{-1}\frac{\partial\boldsymbol{\Gamma}}{\partial\xi_n}\right\} \qquad (11)\end{aligned}$$

where ξ_n refers to the n^{th} entry of $\boldsymbol{\xi}$, $\boldsymbol{\xi} = \{\theta,\phi\}$ is the set of the unknown but deterministic parameters to be estimated, $\text{Re}\{\cdot\}$ symbolizes the real-valued part of the entity inside the curly brackets, $\text{Tr}\{\cdot\}$ represents the trace of the contents inside the curly brackets, and ^{H} denotes conjugate transposition [13], [34], [35], [42].

From (10), $\frac{\partial\boldsymbol{\Gamma}}{\partial\xi_k} = \frac{\partial\boldsymbol{\Gamma}}{\partial\xi_n} = 0$, implying that the second term of (11) vanishes. Inserting (10) in (11) yields

$$\begin{aligned}[\mathbf{F}(\xi)]_{k,n} &= 2\text{Re}\left\{\left[\frac{\partial\boldsymbol{\mu}}{\partial\xi_k}\right]^H\boldsymbol{\Gamma}^{-1}\frac{\partial\boldsymbol{\mu}}{\partial\xi_n}\right\} \\ &= \frac{2}{\sigma_n^2}\text{Re}\left\{\left[\frac{\partial\boldsymbol{\mu}}{\partial\xi_k}\right]^H\frac{\partial\boldsymbol{\mu}}{\partial\xi_n}\right\}. \qquad (12)\end{aligned}$$

With equation (7),

$$\begin{aligned}\left[\frac{\partial\boldsymbol{\mu}}{\partial\xi_k}\right]^H\frac{\partial\boldsymbol{\mu}}{\partial\xi_n} &= \left[\mathbf{s}\otimes\frac{\partial\mathbf{a}(\theta,\phi)}{\partial\xi_k}\right]^H\left[\mathbf{s}\otimes\frac{\partial\mathbf{a}(\theta,\phi)}{\partial\xi_{\mathbf{n}}}\right] \\ &= \mathbf{s}^H\mathbf{s}\left\{\left[\frac{\partial\mathbf{a}(\theta,\phi)}{\partial\xi_k}\right]^H\left[\frac{\partial\mathbf{a}(\theta,\phi)}{\partial\xi_n}\right]\right\} (13)\end{aligned}$$

Using (13) in (12),

$$[\mathbf{F}(\xi)]_{k,n} = 2\frac{\mathbf{s}^H\mathbf{s}}{\sigma_n^2}\text{Re}\left\{\left[\frac{\partial\mathbf{a}(\theta,\phi)}{\partial\xi_k}\right]^H\left[\frac{\partial\mathbf{a}(\theta,\phi)}{\partial\xi_n}\right]\right\} \tag{14}$$

Here,

$$\mathbf{F}(\boldsymbol{\xi}) \quad = \quad \begin{bmatrix}F_{\theta,\theta} & F_{\theta,\phi}\\ F_{\phi,\theta} & F_{\phi,\phi}\end{bmatrix}, \tag{15}$$

from which

$$\begin{bmatrix}\text{CRB}(\theta) & *\\ * & \text{CRB}(\phi)\end{bmatrix} = \begin{bmatrix}F_{\theta,\theta} & F_{\theta,\phi}\\ F_{\phi,\theta} & F_{\phi,\phi}\end{bmatrix}^{-1} \tag{16}$$

where $*$ denotes elements not of interest for the present purpose. From (14),

$$\begin{aligned}[\mathbf{F}(\xi)]_{1,1} &= F_{\theta,\theta} \\ &= 2\frac{\mathbf{s}^H\mathbf{s}}{\sigma_n^2}\text{Re}\left\{\left[\frac{\partial\mathbf{a}(\theta,\phi)}{\partial\theta}\right]^H\left[\frac{\partial\mathbf{a}(\theta,\phi)}{\partial\theta}\right]\right\}, (17)\end{aligned}$$

$$\begin{aligned}[\mathbf{F}(\xi)]_{1,2} &= F_{\theta,\phi} \\ &= 2\frac{\mathbf{s}^H\mathbf{s}}{\sigma_n^2}\text{Re}\left\{\left[\frac{\partial\mathbf{a}(\theta,\phi)}{\partial\theta}\right]^H\left[\frac{\partial\mathbf{a}(\theta,\phi)}{\partial\phi}\right]\right\}, (18)\end{aligned}$$

$$\begin{aligned}[\mathbf{F}(\xi)]_{2,1} &= F_{\phi,\theta} \\ &= 2\frac{\mathbf{s}^H\mathbf{s}}{\sigma_n^2}\text{Re}\left\{\left[\frac{\partial\mathbf{a}(\theta,\phi)}{\partial\phi}\right]^H\left[\frac{\partial\mathbf{a}(\theta,\phi)}{\partial\theta}\right]\right\}, (19)\end{aligned}$$

and

$$\begin{aligned}[\mathbf{F}(\xi)]_{2,2} &= F_{\phi,\phi} \\ &= 2\frac{\mathbf{s}^H\mathbf{s}}{\sigma_n^2}\text{Re}\left\{\left[\frac{\partial\mathbf{a}(\theta,\phi)}{\partial\phi}\right]^H\left[\frac{\partial\mathbf{a}(\theta,\phi)}{\partial\phi}\right]\right\}, (20)\end{aligned}$$

III-C. The Signal

Define $s(m) = \sigma_s \exp\{j(2\pi f m + \varphi)\}$ for $m = 1, 2, 3, \cdots, M$; where φ denotes the signal phase. For M number of time samples, define

$$\mathbf{s} = \sigma_s \left[e^{j(2\pi f+\varphi)},\ e^{j(4\pi f+\varphi)},\ \cdots,\ e^{j(2M\pi f+\varphi)} \right]^T \quad (21)$$

Therefore,

$$\begin{aligned} \mathbf{s}^H \mathbf{s} &= \sigma_s^2 \begin{bmatrix} e^{-j(2\pi f+\varphi)} \\ e^{-j(4\pi f+\varphi)} \\ e^{-j(6\pi f+\varphi)} \\ \vdots \\ e^{-j(2M\pi f+\varphi)} \end{bmatrix}^T \begin{bmatrix} e^{j(2\pi f+\varphi)} \\ e^{j(4\pi f+\varphi)} \\ e^{j(6\pi f+\varphi)} \\ \vdots \\ e^{j(2M\pi f+\varphi)} \end{bmatrix} \\ &= \sigma_s^2 \underbrace{[1+1+1+\cdots+1]}_{M \text{ times}} \\ &= M\sigma_s^2. \end{aligned} \quad (22)$$

III-D. Expansion of the FIM Elements:

We next find the values of $F_{\theta,\theta}$, $F_{\theta,\phi} \equiv F_{\phi,\theta}$, and $F_{\phi,\phi}$ as illustrated below.

From (3),

$$\frac{\partial \mathbf{a}(\theta,\phi)}{\partial \theta} = \begin{bmatrix} \frac{\partial\, \mathbf{a}_{\text{in}}(\theta,\phi)}{\partial \theta} \\ \frac{\partial\, \mathbf{a}_{\text{out}}(\theta,\phi)}{\partial \theta} \end{bmatrix} \quad (23)$$

where the ℓ-th entries of $\frac{\partial\, \mathbf{a}_{\text{in}}(\theta,\phi)}{\partial \theta}$, and $\frac{\partial\, \mathbf{a}_{\text{out}}(\theta,\phi)}{\partial \theta}$ are respectively given by

$$\begin{aligned} \left[\frac{\partial\, \mathbf{a}_{\text{in}}(\theta,\phi)}{\partial \theta}\right]_\ell &= j\frac{2\pi R_{\text{in}}}{\lambda}\cos(\theta)\cos\left(\phi - \frac{2\pi(\ell-1)}{L_{\text{in}}}\right) \\ &\quad \times e^{j\frac{2\pi R_{\text{in}}}{\lambda}\sin(\theta)\cos\left(\phi-\frac{2\pi(\ell-1)}{L_{\text{in}}}\right)}, \end{aligned}$$

for $\ell = 1, 2, \cdots, L_{\text{in}}$; and

$$\begin{aligned} \left[\frac{\partial\, \mathbf{a}_{\text{out}}(\theta,\phi)}{\partial \theta}\right]_\ell &= j\frac{2\pi R_{\text{out}}}{\lambda}\cos(\theta)\cos\left(\phi - \frac{2\pi(\ell-1)}{L_{\text{out}}}\right) \\ &\quad \times e^{j\frac{2\pi R_{\text{out}}}{\lambda}\sin(\theta)\cos\left(\phi-\frac{2\pi(\ell-1)}{L_{\text{out}}}\right)}, \end{aligned}$$

for $\ell = 1, 2, \cdots, L_{\text{out}}$.

Similarly,

$$\frac{\partial \mathbf{a}(\theta,\phi)}{\partial \phi} = \begin{bmatrix} \frac{\partial\, \mathbf{a}_{\text{in}}(\theta,\phi)}{\partial \phi} \\ \frac{\partial\, \mathbf{a}_{\text{out}}(\theta,\phi)}{\partial \phi} \end{bmatrix}, \quad (24)$$

where the ℓ-th entries of $\frac{\partial\, \mathbf{a}_{\text{in}}(\theta,\phi)}{\partial \phi}$, and $\frac{\partial\, \mathbf{a}_{\text{out}}(\theta,\phi)}{\partial \phi}$ are respectively given by

$$\begin{aligned} \left[\frac{\partial\, \mathbf{a}_{\text{in}}(\theta,\phi)}{\partial \phi}\right]_\ell &= -j\frac{2\pi R_{\text{in}}}{\lambda}\sin(\theta)\sin\left(\phi - \frac{2\pi(\ell-1)}{L_{\text{in}}}\right) \\ &\quad \times e^{j\frac{2\pi R_{\text{in}}}{\lambda}\sin(\theta)\cos\left(\phi-\frac{2\pi(\ell-1)}{L_{\text{in}}}\right)}, \end{aligned}$$

for $\ell = 1, 2, \cdots, L_{\text{in}}$; and

$$\begin{aligned} \left[\frac{\partial\, \mathbf{a}_{\text{out}}(\theta,\phi)}{\partial \phi}\right]_\ell &= -j\frac{2\pi R_{\text{out}}}{\lambda}\sin(\theta)\sin\left(\phi - \frac{2\pi(\ell-1)}{L_{\text{out}}}\right) \\ &\quad \times e^{j\frac{2\pi R_{\text{out}}}{\lambda}\sin(\theta)\cos\left(\phi-\frac{2\pi(\ell-1)}{L_{\text{out}}}\right)}, \end{aligned}$$

for $\ell = 1, 2, \cdots, L_{\text{out}}$.

From (23):

$$\begin{aligned} &\left[\frac{\partial \mathbf{a}(\theta,\phi)}{\partial \theta}\right]^H \left[\frac{\partial \mathbf{a}(\theta,\phi)}{\partial \theta}\right] \\ &= \left(\frac{2\pi R_{\text{in}}}{\lambda}\cos(\theta)\right)^2 \underbrace{\sum_{\ell=1}^{L_{\text{in}}} \cos^2\left(\phi - \frac{2\pi(\ell-1)}{L_{\text{in}}}\right)}_{:=\ L_{\text{in}}/2} \\ &\quad + \left(\frac{2\pi R_{\text{out}}}{\lambda}\cos(\theta)\right)^2 \underbrace{\sum_{\ell=1}^{L_{\text{out}}} \cos^2\left(\phi - \frac{2\pi(\ell-1)}{L_{\text{out}}}\right)}_{:=\ L_{\text{out}}/2} \\ &= \left(\frac{2\pi R_{\text{in}}}{\lambda}\cos(\theta)\right)^2 \frac{L_{\text{in}}}{2} + \left(\frac{2\pi R}{\lambda}\cos(\theta)\right)^2 \frac{L_{\text{out}}}{2}. \end{aligned} \quad (25)$$

Using (25) in (17),

$$F_{\theta,\theta} = 4M\left(\frac{\pi}{\lambda}\frac{\sigma_s}{\sigma_n}\right)^2 \left(R_{\text{in}}^2 L_{\text{in}} + R_{\text{out}}^2 L_{\text{out}}\right)\cos^2(\theta) \quad (26)$$

From (24),

$$\begin{aligned} &\left[\frac{\partial \mathbf{a}(\theta,\phi)}{\partial \phi}\right]^H \left[\frac{\partial \mathbf{a}(\theta,\phi)}{\partial \phi}\right] \\ &= \left(\frac{2\pi R_{\text{in}}}{\lambda}\sin(\theta)\right)^2 \underbrace{\sum_{\ell=1}^{L_{\text{in}}} \sin^2\left(\phi - \frac{2\pi(\ell-1)}{L_{\text{in}}}\right)}_{:=\ L_{\text{in}}/2} \\ &\quad + \left(\frac{2\pi R_{\text{out}}}{\lambda}\sin(\theta)\right)^2 \underbrace{\sum_{\ell=1}^{L_{\text{out}}} \sin^2\left(\phi - \frac{2\pi(\ell-1)}{L_{\text{out}}}\right)}_{:=\ L_{\text{out}}/2} \\ &= \left(\frac{2\pi R_{\text{in}}}{\lambda}\sin(\theta)\right)^2 \frac{L_{\text{in}}}{2} + \left(\frac{2\pi R_{\text{out}}}{\lambda}\sin(\theta)\right)^2 \frac{L_{\text{out}}}{2} \end{aligned} \quad (27)$$

Therefore, Using (27) in (20),

$$F_{\phi,\phi} = 4M\left(\frac{\pi}{\lambda}\frac{\sigma_s}{\sigma_n}\right)^2 \left(R_{\text{in}}^2 L_{\text{in}} + R_{\text{out}}^2 L_{\text{out}}\right)\sin^2(\theta) \quad (28)$$

From (23) and (24),

$$\begin{aligned} &\left[\frac{\partial \mathbf{a}(\theta,\phi)}{\partial \theta}\right]^H \left[\frac{\partial \mathbf{a}(\theta,\phi)}{\partial \phi}\right] \\ &= \left(\frac{2\pi R_{\text{in}}}{\lambda}\right)^2 \frac{\sin 2\theta}{4} \underbrace{\sum_{\ell=1}^{L_{\text{in}}} \sin\left(2\phi - \frac{4\pi(\ell-1)}{L_{\text{in}}}\right)}_{:=\ 0} \\ &\quad + \left(\frac{2\pi R_{\text{out}}}{\lambda}\right)^2 \frac{\sin 2\theta}{4} \underbrace{\sum_{\ell=1}^{L_{\text{out}}} \sin\left(2\phi - \frac{4\pi(\ell-1)}{L_{\text{out}}}\right)}_{:=\ 0} \\ &= 0. \end{aligned} \quad (29)$$

Hence, Using (29) in (19),

$$\begin{aligned} F_{\theta,\phi} &= F_{\phi,\theta} \\ &= 0. \end{aligned} \quad (30)$$

III-E. Formulation of the $\mathrm{CRB}(\theta)$ *and* $\mathrm{CRB}(\phi)$ *from the FIM:*

Using (16),

$$\begin{bmatrix} \mathrm{CRB}(\theta) & * \\ * & \mathrm{CRB}(\phi) \end{bmatrix} = \frac{1}{F_{\theta,\theta}F_{\phi,\phi} - F_{\theta,\phi}F_{\phi,\theta}} \begin{bmatrix} F_{\phi,\phi} & -F_{\theta,\phi} \\ -F_{\phi,\theta} & F_{\theta,\theta} \end{bmatrix}. \quad (31)$$

From (31),

$$\begin{aligned} \mathrm{CRB}_{\mathrm{CUCA}}(\theta) &= \frac{F_{\phi,\phi}}{F_{\theta,\theta}F_{\phi,\phi} - F_{\theta,\phi}F_{\phi,\theta}} \\ &= \frac{1}{4\pi^2}\frac{1}{M}\frac{\sec^2(\theta)}{\frac{R_{\mathrm{in}}^2}{\lambda^2}L_{\mathrm{in}} + \frac{R_{\mathrm{out}}^2}{\lambda^2}L_{\mathrm{out}}}\left(\frac{\sigma_n}{\sigma_s}\right)^2 \end{aligned} \quad (32)$$

and

$$\begin{aligned} \mathrm{CRB}_{\mathrm{CUCA}}(\phi) &= \frac{F_{\theta,\theta}}{F_{\theta,\theta}F_{\phi,\phi} - F_{\theta,\phi}F_{\phi,\theta}} \\ &= \frac{1}{4\pi^2}\frac{1}{M}\frac{\csc^2(\theta)}{\frac{R_{\mathrm{in}}^2}{\lambda^2}L_{\mathrm{in}} + \frac{R_{\mathrm{out}}^2}{\lambda^2}L_{\mathrm{out}}}\left(\frac{\sigma_n}{\sigma_s}\right)^2 \end{aligned} \quad (33)$$

Consequently, the $\mathrm{CRB}(\theta)$ and the $\mathrm{CRB}(\phi)$ for the UCA are given by

$$\mathrm{CRB}_{\mathrm{UCA}}(\theta) = \frac{1}{4\pi^2}\frac{1}{M}\frac{\sec^2(\theta)}{\frac{R_{\mathrm{UCA}}^2}{\lambda^2}L_{\mathrm{UCA}}}\left(\frac{\sigma_n}{\sigma_s}\right)^2, \quad (34)$$

and

$$\mathrm{CRB}_{\mathrm{UCA}}(\phi) = \frac{1}{4\pi^2}\frac{1}{M}\frac{\csc^2(\theta)}{\frac{R_{\mathrm{UCA}}^2}{\lambda^2}L_{\mathrm{UCA}}}\left(\frac{\sigma_n}{\sigma_s}\right)^2. \quad (35)$$

IV RESULTS ANALYSIS AND DISCUSSION

The CUCA's CRBs in (32) - (33) differ from the UCA's CRBs in (34) - (35) by the terms, $\frac{1}{R_{\mathrm{in}}^2 L_{\mathrm{in}} + R_{\mathrm{out}}^2 L_{\mathrm{out}}}$ and $\frac{1}{R_{\mathrm{UCA}}^2 L_{\mathrm{UCA}}}$. Suppose there is a constraint of $L_{\mathrm{UCA}} = L_{\mathrm{in}} + L_{\mathrm{out}}$. Then, the smallest value of L_{UCA} can be found such that the UCA and the CUCA have the same performance and as a result, the corresponding value of R_{UCA} computed. Now, suppose that $L_{\mathrm{UCA}} = L_{\mathrm{out}}$ then clearly, it implies that $L_{\mathrm{in}} = 0$. Since for the UCA and the CUCA to perform the same we have the equation $R_{\mathrm{UCA}}^2 L_{\mathrm{UCA}} = R_{\mathrm{in}}^2 L_{\mathrm{in}} + R_{\mathrm{out}}^2 L_{\mathrm{out}}$, then the corresponding value of R_{UCA} could be given by,

$$R_{\mathrm{UCA}} = +\sqrt{\frac{R_{\mathrm{out}}^2 L_{\mathrm{out}}}{L_{\mathrm{UCA}}}}.$$

Moreover, we note that, the UCA and the CUCA have equal performance when the ratio of their CRBs is one and thus we have the equation:

$$R_{\mathrm{UCA}}^2 L_{\mathrm{UCA}} = \left(R_{\mathrm{in}}^2 - R_{\mathrm{out}}^2\right) L_{\mathrm{in}} + R_{\mathrm{out}}^2 L_{\mathrm{UCA}},$$

which can also be written as;

$$\left(R_{\mathrm{UCA}}^2 - R_{\mathrm{out}}^2\right) L_{\mathrm{UCA}} = \left(R_{\mathrm{in}}^2 - R_{\mathrm{out}}^2\right) L_{\mathrm{in}},$$

implying that,

$$\frac{L_{\mathrm{in}}}{L_{\mathrm{UCA}}} = \frac{R_{\mathrm{UCA}}^2 - R_{\mathrm{out}}^2}{R_{\mathrm{in}}^2 - R_{\mathrm{out}}^2}.$$

Therefore, the UCA and the CUCA performs the same, if, $R_{\mathrm{UCA}} = R_{\mathrm{in}}$ and $L_{\mathrm{UCA}} = L_{\mathrm{in}}$ implying that $L_{\mathrm{out}} = 0$ since $L_{\mathrm{UCA}} = L_{\mathrm{in}} + L_{\mathrm{out}}$.

In addition, the CRBs would be smallest, if all sensors are placed on the outer circle (i.e. $L_{\mathrm{in}} = 0$) and $R_{\mathrm{UCA}} = R_{\mathrm{out}} \rightarrow \infty$.

IV-A. Special Cases

IV-A.1. If $R_{\mathrm{in}} = (R_{\mathrm{out}} - \frac{\lambda}{2})$*:* Equations (32) and (33) for the $\mathrm{CRB}(\theta)$ and the $\mathrm{CRB}(\phi)$ of the CUCA respectively become

$$\mathrm{CRB}_{\mathrm{CUCA}}(\theta) \quad (36)$$
$$= \frac{1}{4\pi^2}\frac{1}{M}\left(\frac{\sigma_n}{\sigma_s}\right)^2 \frac{\sec^2(\theta)}{\frac{R_{\mathrm{out}}^2}{\lambda^2}\left(L_{\mathrm{in}} + L_{\mathrm{out}}\right) + \left(\frac{1}{4} - \frac{R_{\mathrm{out}}}{\lambda}\right) L_{\mathrm{in}}},$$

$$\mathrm{CRB}_{\mathrm{CUCA}}(\phi) \quad (37)$$
$$= \frac{1}{4\pi^2}\frac{1}{M}\left(\frac{\sigma_n}{\sigma_s}\right)^2 \frac{\csc^2(\theta)}{\frac{R_{\mathrm{out}}^2}{\lambda^2}\left(L_{\mathrm{in}} + L_{\mathrm{out}}\right) + \left(\frac{1}{4} - \frac{R_{\mathrm{out}}}{\lambda}\right) L_{\mathrm{in}}}.$$

IV-A.2. If furthermore $L_{\mathrm{in}} = 4$ *and* $L_{\mathrm{out}} = L_{\mathrm{UCA}} - 4$*:* Equations (36) and (37) become

$$\mathrm{CRB}_{\mathrm{CUCA}}(\theta) = \frac{1}{4\pi^2}\frac{1}{M}\frac{\sec^2(\theta)}{\frac{R_{\mathrm{out}}^2}{\lambda^2}L_{\mathrm{UCA}} - 4\frac{R_{\mathrm{out}}}{\lambda} + 1}\left(\frac{\sigma_n}{\sigma_s}\right)^2, \quad (38)$$

$$\mathrm{CRB}_{\mathrm{CUCA}}(\phi) = \frac{1}{4\pi^2}\frac{1}{M}\frac{\csc^2(\theta)}{\frac{R_{\mathrm{out}}^2}{\lambda^2}L_{\mathrm{UCA}} - 4\frac{R_{\mathrm{out}}}{\lambda} + 1}\left(\frac{\sigma_n}{\sigma_s}\right)^2. \quad (39)$$

IV-B. The Proposed Geometry

Imposed on the aforementioned 2-circle concentric and uniform array geometry are these additional constraints:
(i) $R_{\text{out}} = R_{\text{in}} + \frac{\lambda}{2}$.
(ii) L_{out} is wholly divisible by 4.
(iii) $L_{\text{in}} = 4$.

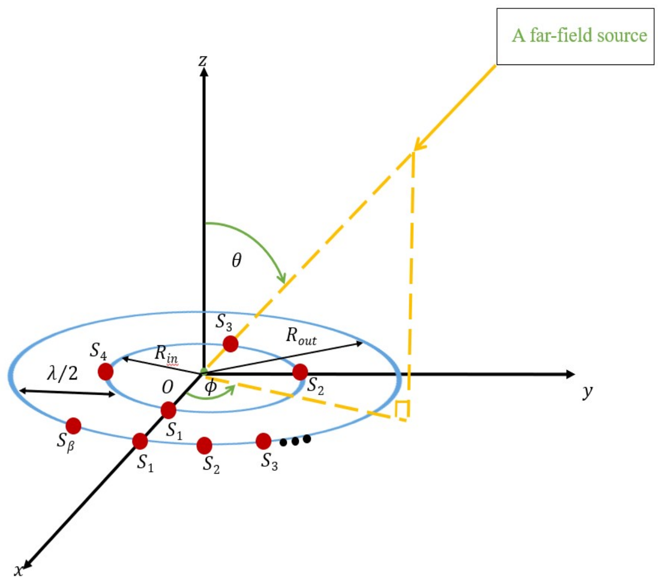

Fig. 3. The Proposed Geometry. Here, β denotes $L_{\text{UCA}} - 4$

Constraints (ii)-(iii) together produce four pairs of half-wavelength-spaced sensors, with one pair each along the positive x-axis, the negative x-axis, the positive y-axis, and the negative y-axis.

The above ensures (a) half-wavelength spacing along each of the two Cartesian dimensions of the present planar array grid, (b) circular symmetry about the Cartesian origin, (c) a maximum number of sensors on the outer circle.

Using the constraints in section IV-B:

$$\begin{aligned} & (2\pi)^2 M \left(\frac{\sigma_s}{\sigma_n}\right)^2 \cos^2(\theta)\mathrm{CRB}_{\text{CUCA}}(\theta) \\ = & \frac{1}{(L_{\text{out}}+4)\left(\frac{R_{\text{out}}}{\lambda}\right)^2 - 4\frac{R_{\text{out}}}{\lambda} + 1} := \tilde{\mathrm{CRB}}_{\text{CUCA}} \\ \equiv & (2\pi)^2 M \left(\frac{\sigma_s}{\sigma_n}\right)^2 \sin^2(\theta)\mathrm{CRB}_{\text{CUCA}}(\phi). \end{aligned} \quad (40)$$

Since $R_{\text{in}} \geq 0$, then from constraint (i), $R_{\text{out}} \geq \frac{\lambda}{2}$ which implies that $\frac{R_{\text{out}}}{\lambda} \geq \frac{1}{2}$.

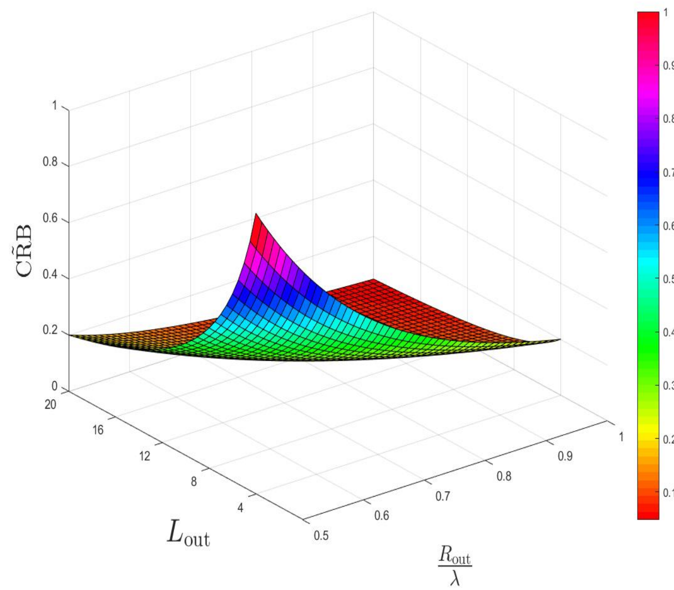

Fig. 4. Variation of the CRBs with respect to $\frac{R_{\text{out}}}{\lambda}$ and L_{out}. Refer to (40).

From Figure 4, it is clear that the CRBs decrease with increase in L_{out} and/or $\frac{R_{\text{out}}}{\lambda}$, which is expected. Analytical explanation to this observation is given below.

From the graph on Figure 4, the turning point with respect to R_{out} using (40) is given by

$$\begin{aligned} \frac{\partial \tilde{\mathrm{CRB}}_{\text{CUCA}}}{\partial R_{\text{out}}} &= \frac{-2(L_{\text{out}}+4)\frac{R_{\text{out}}}{\lambda} + 4}{\left((L_{\text{out}}+4)\left(\frac{R_{\text{out}}}{\lambda}\right)^2 - 4\frac{R_{\text{out}}}{\lambda} + 1\right)^2} \\ &= 0, \end{aligned}$$

which implies that the turning point occurs when

$$\frac{R_{\text{out}}}{\lambda} = \frac{2}{L_{\text{out}}+4}.$$

However, since $L_{\text{out}} > 0$, then $\frac{R_{\text{out}}}{\lambda} \leq 0.5$ which is the minimum point of $\frac{R_{\text{out}}}{\lambda}$ in Figure 4. Hence the graph has no turning point with respect to $\frac{R_{\text{out}}}{\lambda}$ and thus $\tilde{\mathrm{CRB}}_{\text{CUCA}}$ decreases with increase in $\frac{R_{\text{out}}}{\lambda}$.

This observation is also clear from (40) since the numerator is a constant, and the denominator $L_{\text{out}}\left(\frac{R_{\text{out}}}{\lambda}\right)^2 + 4\left(\frac{R_{\text{out}}}{\lambda}\right)^2 - 4\frac{R_{\text{out}}}{\lambda} + 1 \gg 1$ as $\frac{R_{\text{out}}}{\lambda}$ increases.

Similarly, the turning point with respect to L_{out} is given by

$$\begin{aligned} \frac{\partial \tilde{\mathrm{CRB}}_{\text{CUCA}}}{\partial L_{\text{out}}} &= \frac{-\left(\frac{R_{\text{out}}}{\lambda}\right)^2}{\left((L_{\text{out}}+4)\left(\frac{R_{\text{out}}}{\lambda}\right)^2 - 4\frac{R_{\text{out}}}{\lambda} + 1\right)^2} \\ &= 0, \end{aligned}$$

which implies that the turning point occurs when

$$\frac{R_{\text{out}}}{\lambda} = 0,$$

which is infeasible since $\frac{R_{\text{out}}}{\lambda} \geq 0.5$. Hence the graph has no turning point with respect to L_{out} and thus $\tilde{\mathrm{CRB}}_{\text{CUCA}}$ decreases with increase in L_{out}.

This observation is also clear from (40) since the numerator is a constant, and the denominator $L_{\text{out}}\left(\frac{R_{\text{out}}}{\lambda}\right)^2 + 4\left(\frac{R_{\text{out}}}{\lambda}\right)^2 - 4\frac{R_{\text{out}}}{\lambda} + 1 \gg 1$ as L_{out} increases.

IV-B.1. A Single-Circle: For a single-circle with $\frac{\lambda}{2}$ inter-sensor spacing with L number of sensors we have

$$L_{\text{UCA}} \;=\; \frac{\pi}{\sin^{-1}\left(\frac{\lambda}{4R_{\text{UCA}}}\right)}.$$

Using equations (34) – (35) we obtain

$$\begin{aligned} & (2\pi)^2 M \left(\frac{\sigma_s}{\sigma_n}\right)^2 \cos^2(\theta)\mathrm{CRB}_{\text{UCA}}(\theta) \\ = \;& \frac{1}{\left(\frac{R_{\text{UCA}}}{\lambda}\right)^2 L_{\text{UCA}}} \;:=\; \tilde{\mathrm{CRB}}_{\text{UCA}} \qquad (41) \\ \equiv \;& (2\pi)^2 M \left(\frac{\sigma_s}{\sigma_n}\right)^2 \sin^2(\theta)\mathrm{CRB}_{\text{UCA}}(\phi). \end{aligned}$$

IV-B.2. A 2-Circle Array: For a 2-circle geometry where

a) each circle has L number of sensors,
b) the 2-circles radii differ by $\frac{\lambda}{2}$ (i.e $R_{\text{out}} = R_{\text{in}} + \frac{\lambda}{2}$), and
c) each sensor on the outer circle is matched with one sensor on the inner circle.

Using the above information and equations (32) – (33) yields

$$\begin{aligned} & (2\pi)^2 M \left(\frac{\sigma_s}{\sigma_n}\right)^2 \cos^2(\theta)\mathrm{CRB}_{\text{CUCA}}(\theta) \\ = \;& \frac{1}{2\left(\frac{R_{\text{in}}}{\lambda}\right)^2 + \frac{R_{\text{in}}}{\lambda} + \frac{1}{4}}\frac{1}{L} \;:=\; \tilde{\mathrm{CRB}}_{\text{CUCA}} \qquad (42) \\ \equiv \;& (2\pi)^2 M \left(\frac{\sigma_s}{\sigma_n}\right)^2 \sin^2(\theta)\mathrm{CRB}_{\text{CUCA}}(\phi). \end{aligned}$$

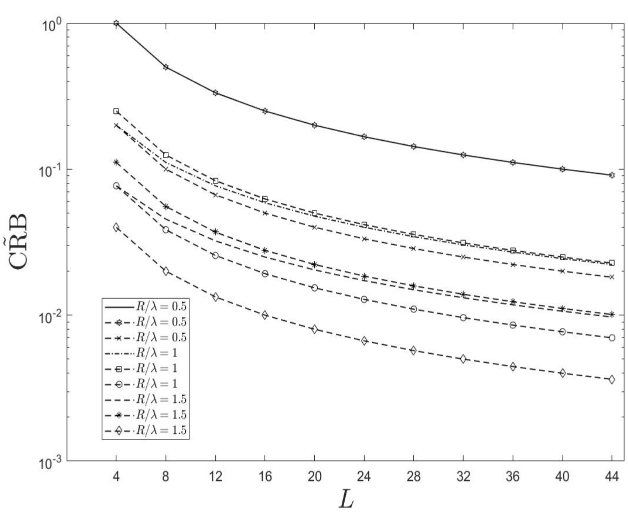

Fig. 5. $\tilde{\mathrm{CRB}}$ of the proposed geometry where: $R_{\text{out}} = R_{\text{in}} + \frac{\lambda}{2}$, L_{out} is wholly divisible by 4, and $L_{\text{in}} = 4$ using (40), the single-circle with $\frac{\lambda}{2}$ inter-sensor spacing and with L number of sensors using (41), and the 2-circle geometry where: each circle has L number of sensors, the 2-circles radii differ by $\frac{\lambda}{2}$ (i.e $R_{\text{out}} = R_{\text{in}} + \frac{\lambda}{2}$), and each sensor on the outer circle is matched with one sensor on the inner circle using (42)

From Figure 5, it can be generally deduced that, the CRBs for all the three geometries decrease gently with increase in the number of sensors (L) at different values of $\frac{R_{\text{out}}}{\lambda}$. However, the proposed geometry (the solid, the dashed-dot and the dashed curves) and the single-circle geometry (the dashed-hexagon, the dashed-square, and dashed-asteriks curves) with L number of sensors have exactly equal performance at $\frac{R_{\text{out}}}{\lambda} = 0\cdot 5$ but thereafter, the proposed geometry has lower CRB for all $\frac{R_{\text{out}}}{\lambda} > 0\cdot 5$.

Importantly, of all the three geometries, the 2-circle geometry (the dashed-cross, the dashed-circle and the dashed-diamond curves) has the lowest CRBs for all values of $\frac{R_{\text{out}}}{\lambda}$.

In all the geometries, increase in $\frac{R_{\text{out}}}{\lambda}$ reduces the CRBs. This is due to increased aperture.

IV-C. Further Comparisons

Define $L_{\text{tot}} = L_{\text{out}} + L_{\text{in}}$ and consider the following cases.

IV-C.1. Case 1: A single circle with half-wavelength inter-sensor spacing, i.e. $2R_{\text{out}}\sin\left(\frac{\pi}{L_{\text{UCA}}}\right) = \frac{\lambda}{2}$*.:* Then, (34)-(35) become

$$\begin{aligned} \tilde{\mathrm{CRB}} \;&:=\; (2\pi)^2 M \left(\frac{\sigma_s}{\sigma_n}\right)^2 \cos^2(\theta)\mathrm{CRB}(\theta) \\ &=\; (2\pi)^2 M \left(\frac{\sigma_s}{\sigma_n}\right)^2 \sin^2(\theta)\mathrm{CRB}(\phi) \\ &=\; \frac{1}{\left(\frac{R_{\text{UCA}}}{\lambda}\right)^2 L_{\text{tot}}}. \qquad (43) \end{aligned}$$

IV-C.2. Case 2: The 2-ring grid proposed in Section IV-B: Here, R_{out} and $L_{\text{out}} = L_{\text{tot}} - 4$ and $\frac{R_{\text{in}}}{\lambda} = \frac{R_{\text{out}}}{\lambda} - \frac{1}{2}$. So, (38)-(39) yield

$$\begin{aligned} \tilde{\mathrm{CRB}} \;&:=\; (2\pi)^2 M \left(\frac{\sigma_s}{\sigma_n}\right)^2 \cos^2(\theta)\mathrm{CRB}(\theta) \\ &=\; (2\pi)^2 M \left(\frac{\sigma_s}{\sigma_n}\right)^2 \sin^2(\theta)\mathrm{CRB}(\phi) \\ &=\; \frac{1}{\frac{R_{\text{out}}^2}{\lambda^2}L_{\text{tot}} - 4\frac{R_{\text{out}}}{\lambda} + 1}. \qquad (44) \end{aligned}$$

IV-C.3. Case 3: A 2-ring CUCA, with:

a) $\frac{R_{\text{in}}}{\lambda} = \frac{R_{\text{out}}}{\lambda} - \frac{1}{2}$
b) $L_{\text{out}} = L_{\text{in}}$ implying that L_{out} and L_{in} have the same polar azimuth on the x-y plane.

Using the constraints in (32)-(33),

$$\begin{aligned} \tilde{\mathrm{CRB}} \;&:=\; (2\pi)^2 M \left(\frac{\sigma_s}{\sigma_n}\right)^2 \cos^2(\theta)\mathrm{CRB}(\theta) \\ &=\; (2\pi)^2 M \left(\frac{\sigma_s}{\sigma_n}\right)^2 \sin^2(\theta)\mathrm{CRB}(\phi) \\ &=\; \frac{1}{L_{\text{tot}}}\left[2\left(\frac{R_{\text{out}}}{\lambda}\right)^2 - \frac{R_{\text{out}}}{\lambda} + \frac{1}{4}\right]^{-1} \qquad (45) \end{aligned}$$

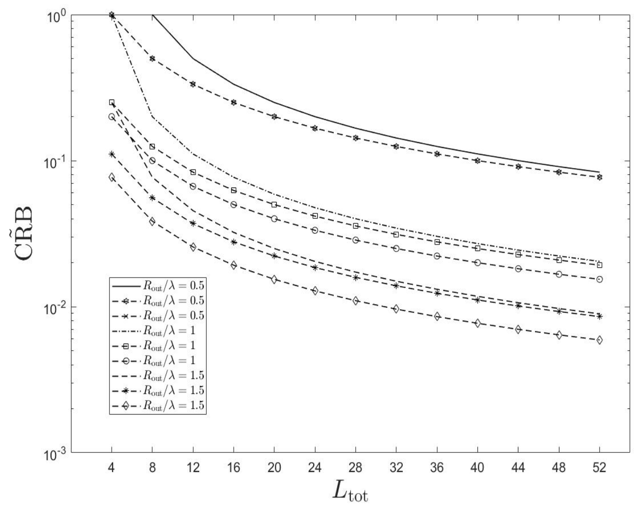

Fig. 6. $\tilde{\mathrm{CRB}}$ of the single circle with half-wavelength inter-sensor spacing using (43), the 2-ring grid proposed in IV-B using (44), and the 2-ring CUCA, with $\frac{R_{\mathrm{in}}}{\lambda} = \frac{R_{\mathrm{out}}}{\lambda} - \frac{1}{2}$ and $L_{\mathrm{out}} = L_{\mathrm{in}}$ using (45).

Summary

Refer to Figure 6.

Case 1 (the single circle with half-wavelength inter-sensor spacing): Represented by the dashed-hexagon, the dashed-square and the dashed-star curves, for different values of R_{out}/λ.

Case 2 (the 2-ring grid proposed in IV-B): Represented by the solid, the dashed-dot and the dashed curves, for different values of R_{out}/λ.

Case 3 (the 2-ring CUCA, with $\frac{R_{\mathrm{in}}}{\lambda} = \frac{R_{\mathrm{out}}}{\lambda} - \frac{1}{2}$ and $L_{\mathrm{out}} = L_{\mathrm{in}}$): Represented by dash-cross, the dashed-circle and the dashed-diamond curves, for different values of R_{out}/λ.

Observations

1) Case 3 moves away from Case 1 as R_{out}/λ increases.
2) Case 3 moves away from Case 1 as L_{tot} increases.
3) Case 2 approaches Case 1 as L_{tot} increases.
4) Case 2 has the highest CRB values for all R_{out}/λ.
5) Case 3 has the lowest CRB values for $R_{\mathrm{out}}/\lambda > 0.5$.

IV-D. Numerical Case

As aforementioned, the CUCA's and the UCA's CRBs in (32) - (33) and (34) - (35) respectively differ by the terms, $\frac{1}{R_{\mathrm{in}}^2 L_{\mathrm{in}} + R_{\mathrm{out}}^2 L_{\mathrm{out}}}$ and $\frac{1}{R_{\mathrm{UCA}}^2 L_{\mathrm{UCA}}}$. Now, with the strategy of enlarging array's aperture, $R_{\mathrm{out}} >> R_{\mathrm{UCA}}$ implying that $R_{\mathrm{in}} + R_{\mathrm{out}} >> R_{\mathrm{UCA}}$. Also $R_{\mathrm{in}} L_{\mathrm{in}} + R_{\mathrm{out}} L_{\mathrm{out}} > R_{\mathrm{UCA}} L_{\mathrm{UCA}}$ since $L_{\mathrm{UCA}} = L_{\mathrm{in}} + L_{\mathrm{out}}$ which implies that $\frac{1}{R_{\mathrm{in}}^2 L_{\mathrm{in}} + R_{\mathrm{out}}^2 L_{\mathrm{out}}} < \frac{1}{R_{\mathrm{UCA}}^2 L_{\mathrm{UCA}}}$. For example, suppose we choose $R_{\mathrm{out}} = 20$ units, $R_{\mathrm{in}} = 8$ units, $R_{\mathrm{UCA}} = 12$ units, $L_{\mathrm{UCA}} = 12$, $L_{\mathrm{out}} = 8$ and $L_{\mathrm{in}} = 4$ arbitrarily. Substituting these values in $\frac{1}{R_{\mathrm{in}}^2 L_{\mathrm{in}} + R_{\mathrm{out}}^2 L_{\mathrm{out}}}$ and $\frac{1}{R_{\mathrm{UCA}}^2 L_{\mathrm{UCA}}}$ respectively, then we find that $\frac{1}{R_{\mathrm{in}}^2 L_{\mathrm{in}} + R_{\mathrm{out}}^2 L_{\mathrm{out}}} = \frac{1}{3456}$ and $\frac{1}{R_{\mathrm{UCA}}^2 L_{\mathrm{UCA}}} = \frac{1}{1728}$ which clearly implies that $\frac{1}{R_{\mathrm{in}}^2 L_{\mathrm{in}} + R_{\mathrm{out}}^2 L_{\mathrm{out}}} < \frac{1}{R_{\mathrm{UCA}}^2 L_{\mathrm{UCA}}}$. This numerical example and any other example satisfying the above conditions further verifies that the 2-circle concentric uniform array has lower CRB than the single ring array and therefore has better performance.

V Conclusion

A new concentric circular sensor-array grid termed as the 2-circle concentric array geometry that increases the array's spatial aperture while maintaining only half a wavelength inter-sensor spacing is proposed. A better-accurate performance in direction finding of the proposed array grid over a single ring array geometry termed as uniform circle array (UCA) has been analytically verified via Cramér-Rao bound analysis. Further, the performance in direction finding of the proposed array grid and that of a single ring array termed as the uniform circular array has been compared graphically under different constraints of investigation. It has been found that, the Cramér-Rao bound decreases with increase in the number of sensors and/or the radii (increase in array's spatial aperture). The proposed array grid has been found to have the lowest CRB and thus has better estimation accuracy than the single ring array.

References

[1] H. L. Van Trees, *Detection, Estimation and Modulation Theory, Part IV: Optimum Array Processing*, New York, USA: John Wiley and Sons, 2002.

[2] D. Kajaree and R. Behera, "A survey on web crawler approaches," *International Journal of Innovative Research in Computer and Communication Engineering*, vol. 5, no. 2, pp. 1302-1309, 2017.

[3] M. Devendra and K. Manjunathachari, "Solar DC microgrid for rural electrification: A case study," *International Advanced Research Journal in Science, Engineering and Technology (IARJSET)*, vol. 2, no. 1, pp. 1-5, 2015.

[4] S. Rhode, "Introduction into theory of direction finding, radiomonitoring and radiolocation," *International Journal of Computer Applications* ,vol. 6, no. 3, pp.26-49, August 2010.

[5] V. Krishnaveni, T. Kesavamurthy, and B. Aparna. "Beamforming for direction-of-arrival (DOA) estimation-a survey," *International Journal of Computer Applications*, vol. 61, no. 11, January 2013.

[6] S. A. Vorobyov, A. B. Gershman, and K. M. Wong "Maximum likelihood direction-of-arrival estimation in unknown noise fields using sparse sensor arrays," *IEEE Transactions on Signal Processing*, vol. 53, no. 1, pp. 34-43, January 2005.

[7] K. T. Wong and M. D. Zoltowski, "Self-initiating MUSIC-based direction finding and polarization estimation in spatio-polarizational beamspace," *IEEE Transactions on Antennas and Propagation*, vol. 48, no. 8, pp. 1235-1245, august 2000.

[8] M. J. Abedin and A. S. Mohan, "Maximum likelihood near field localisation using concentric circular ring array." *IEEE International Conference on In Electromagnetics in Advanced Applications*, pp. 533-536, September 2010.

[9] M. D. Zoltowski and K. T. Wong, "ESPRIT-based 2-D direction finding with a sparse uniform array of electromagnetic vector sensors," *IEEE Transactions on Signal Processing*, vol. 48, no. 8, pp. 2195-2204, August 2000.

[10] B. Friedlander, *Wireless direction-finding fundamentals in classical and modern direction-of-arrival estimation*, pp. 1-51, Elsevier 2009.

[11] D. M. Kitavi, T. Hao, and K. T. Wong, "A regular tetrahedral array whose constituent sensors fail randomlyA lower bound for direction-of-arrival estimation," *IEEE conference on Antennas and Propagation*, pp. 1-5., November 2016.

[12] N. Tayem and H. M. Kwon, "L-shape 2-dimensional arrival angle estimation with propagator method," *IEEE transactions on antennas and propagation*, vol. 53, no. 5, pp. 1622-1630, May 2005.

[13] D. M. Kitavi, K. T. Wong, and C.-C. Hung, "An L-Shaped Array With Nonorthogonal AxesIts CramrRao Bound for Direction Finding," *IEEE Transactions on Aerospace and Electronic Systems*, vol. 54, no. 1, pp. 486-492, February 2017.

[14] R. L. Haupt, "Optimized element spacing for low sidelobe concentric ring arrays," *IEEE Transactions on Antennas and Propagation*, vol. 56, no. 1, pp. 266-268, January 2008.

[15] U. Singh, and T. S. Kamal, “Synthesis of thinned planar concentric circular antenna arrays using biogeography-based optimisation,” *IET microwaves, antennas and propagation*, vol. 6, no. 7, pp. 822-829, May 2012.

[16] L. Zhang, Y.-C. Jiao, B. Chen and Z.-B. Weng, “Design of Wideband Concentric-Ring Arrays with Three-Dimensional Beam Scanning Based on the Optimization of Array Geometry,” *Electromagnetics*, vol. 32, no. 6, pp. 305-320, July 2012.

[17] Y. Jiang and S. Zhang, “An innovative strategy for synthesis of uniformly weighted circular aperture antenna array based on the weighting density method,” *IEEE Antennas and Wireless Propagation Letters*, vol. 12, pp. 725-728, May 2013.

[18] L. Wang, G. Wang, and Z. Chen, “Joint DOA-polarization estimation based on uniform concentric circular array,” *Journal of Electromagnetic Waves and Applications*, vol. 27, no. 13, pp. 1702-1714, September 2013.

[19] G. Ram, D. Mandal, R. Kar, and S. P. Ghoshal, “Circular and concentric circular antenna array synthesis using cat swarm optimization,” *IETE Technical Review*, vol. 32, no. 3, pp. 204-217, May 2015.

[20] X. Zhao, Y. Zhang and Q. Yang, “Synthesis of sparse concentric ring arrays based on Bessel function,” *IET Microwaves, Antennas and Propagation*, vol. 11, no. 11, pp. 1651-1660, June 2017.

[21] K. T. Wong and M. D. Zoltowski, “Extended-aperture underwater acoustic multisource azimuth/elevation direction-finding using uniformly but sparsely spaced vector hydrophones,” *IEEE Journal of Oceanic Engineering*, vol. 22, no. 4, pp. 659-672, October 1997.

[22] K. T. Wong, S. Yang, J. F. Caleb, K. Salman, and T. Wai-Yip, “Electrically Long Dipoles in a Collocated/Orthogonal Triadfor Direction Finding and Polarization Estimation,” *IEEE Transactions on Antennas and Propagation*, vol. 65, no. 11, pp. 6057-6067, November 2017.

[23] K. T. Wong, J. N. Chibuzo, and I. W. Yue, “A triad of cardioid sensors in orthogonal orientation and spatial collocationIts spatial-matched-filter-type beam-pattern,” *IEEE Transactions on Signal Processing*, vol. 66, no. 4, pp. 895-906, February 2018.

[24] S. Khan, K. T. Wong, S. Yang, and T. Wai-Yip, “Electrically Large Circular Loops in the Estimation of an Incident Emitters Direction-of-Arrival or Polarization,” *IEEE Transactions on Antennas and Propagation*, vol. 66, no. 6, pp. 3046-3055, June 2018.

[25] T. G. Spence and H. W. Douglas, “Design of broadband planar arrays based on the optimization of aperiodic tilings,” *IEEE Transactions on Antennas and Propagation*, vol. 56, no. 1, pp. 76-86, January 2008.

[26] M. Alvarez-Folgueiras, A. R.-G. Juan, and A.-P. Francisco, “High-performance uniformly excited linear and planar arrays based on linear semiarrays composed of subarrays with different uniform spacings,” *IEEE Transactions on Antennas and Propagation*, vol. 57, no. 12, pp. 4002-4006, December 2009.

[27] M. D. Gregory, F. A. Namin, and D. H. Werner, “Exploiting rotational symmetry for the design of ultra-wideband planar phased array layouts,” *IEEE Transactions on Antennas and Propagation*, vol. 61, no. 1, pp. 176-184, January 2013.

[28] K. Chen, H. Chen, L. Wang, and H. Wu, “Modified real ga for the synthesis of sparse planar circular arrays,” *IEEE Antennas Wirel. Propag. Lett.*, vol. 15, pp. 274-277, January 2016.

[29] M. G. Pralon, G. Del-Galdo, M. Landmann, M. A. Hein, and R. S. Thoma, “Suitability of compact antenna arrays for direction-of-arrival estimation,” *IEEE Transaction on Antenna and Propagation*, no. 65, vol. 12, pp. 7244-7256, December 2017.

[30] H. Sun, W. Y. Chiu,J. Jiang, A. Nallanathan, and H. V. Poor, “Wideband spectrum sensing with sub-Nyquist sampling in cognitive radios,” *IEEE Transaction on Signal Processing*, no. 60, vol. 11, pp. 6068-6073, November 2012.

[31] B. A. Olshausen, “Aliasing,” *Sensory Processes*, pp. 3-4, October 2000.

[32] M. D. Zoltowski, and C. P. Mathews, “Real-time frequency and 2-D angle estimation with sub-Nyquist Ssatio-temporal sampling,” *IEEE Transaction on Signal Processing*, no. 42, vol. 10, pp. 2781-2794, October 1994.

[33] S. M. Kay, *Fundamental of Statistical Signal Processing: Estimation Theory*, Upper Saddle River, New Jersey, USA: Prentice Hall, 1993.

[34] D. M. Kitavi, T.-C. Lin, K. T. Wong, and Y. I. Wu, “Direction finding with the sensors gains suffering Bayesian uncertainty - hybrid CRB and MAP estimation,” *IEEE Transactions on Aerospace and Electronic Systems*, vol. 52, no. 4, pp. 2038-2044, August 2016.

[35] D. M. Kitavi, K. T. Wong, M. Zou, and K. Agrawal, “A lower bound of the estimation error of an emitter’s direction of arrival/polarization for collocated triad of orthogonal dipoles/loops that fail randomly,” *IET Microwaves, Antennas, and Propagation*, vol. 11, no. 7, pp. 961-970, June 2017.

[36] C. Hui and B. Zheng, “Performance analysis of self-calibration algorithm for concentric-UCA,” *IEEE International Conference on Wireless Communications and Signal Processing*, pp. 1-5, October 2010.

[37] S. Akkar, F. Harabi and A. Gharsallah, “Concentric circular-shaped electronically steerable parasitic array radiator antennas for full-azimuth directions of arrival estimation with reduced computational load,” *IET microwaves, antennas and propagation*, vol. 6, no. 11, pp. 1236-1243, August 2012.

[38] D. T. Vu, R. Alexandre, B. Rmy, and M. Sylvie, “A Cramr Rao bounds based analysis of 3D antenna array geometries made from ULA branches,” *Multidimensional Systems and Signal Processing*, vol. 24, no. 1, pp. 121-155, March 2013.

[39] B. Liao, K.-M. Tsui, and S.-C. Chan, “Frequency invariant uniform concentric circular arrays with directional elements,” *IEEE Transactions on Aerospace and Electronic Systems*, vol. 49, no. 2, pp. 871-884, April 2013.

[40] P. H. Leong, T. D. Abhayapala and T. A. Lamahewa, “Multiple target localization using wideband echo chirp signals,” *IEEE Transactions on Signal Processing*, vol. 61, no. 16, pp. 4077-4089, August 2013.

[41] J. P. Delmas, “Performance bounds and statistical Analysis of DOA estimation,” *In Academic Press Library in Signal Processing*, vol. 3, pp. 719-764. Elsevier, 2014.

[42] D. M. Kitavi, T.-C. Lin, and K. T. Wong, “A tetrahedral array of isotropic sensors, each suffering a random complex gainthe resulting hybrid Cramr-Rao bound for direction finding,” *IEEE national conference On Aerospace and Electronics Conference (NAECON) and Ohio Innovation Summit (OIS)*, pp. 412-415, July 2016.

[43] H. Gazzah, J. P. Delmas, and M. J. L. Sergio, “Direction-finding arrays of directional sensors for randomly located sources,” *IEEE Transactions on Aerospace and Electronic Systems*, vol. 52, no. 4, pp. 1995-2003, August 2016.

Musyoka KINYILI obtained the B.Sc. (first-class honours) in Mathematics and Biology in 2017 from the University of Embu (Kenya) and currently pursuing Master of Science in Applied Mathematics at the University of Embu (Kenya).

Dominic Makaa KITAVI obtained the B.Sc. (first-class honours) in Mathematics in 2011 from the University of Nairobi (Kenya), M.Sc. (cum laude) in Mathematical Sciences in 2013 from the University of Western Cape (South Africa), and Ph.D. in Electronic and Information Engineering, at the Hong Kong Polytechnic University (Hong Kong) in 2017.

D. M. Kitavi also obtained Certified Public Accountant one (CPA 1) from KASNEB (Kenya) in 2008.

D. M. Kitavi was an Accounts Assistant in Twiga Chemical Industries Limited (Nairobi, Kenya) in 2011-2012, and Assistant Lecturer at Mount Kenya University (Mombasa, Kenya) in 2014. Since September 2017, D. M. Kitavi has been with the University of Embu (Kenya) as a Lecturer.

D. M. Kitavi’s research interest lies in statistical signal processing and partial differential equations.

Cyrus Gitonga NGARI obtained a second class honours (upper division) in B.ED (Science) - Double Mathematics, in 2005 from Egerton University (Kenya), M.Sc. in Applied Mathematics in 2013 from Kenyatta University (Kenya), and Ph.D. in Applied Mathematics from Moi University (Kenya) in 2017.

C. G. Ngari also obtained Certified Public Accountant one (CPA 1) from KASNEB (Kenya).

C. G. Ngari has twelve years teaching experience at Secondary school level and five years experience at university level. Since January 2018, C. G. Ngari has been with the University of Embu (Kenya) as a Lecturer.

C. G. Ngari's research interest lies in Mathematical Modelling, Analysis and Simulations.